Localized matter-wave patterns with attractive interaction in rotating potentials

Hidetsugu Sakaguchi[1] and Boris A. Malomed[2]

[1]*Department of Applied Science for Electronics and Materials, Interdisciplinary Graduate School of Engineering Sciences, Kyushu University, Kasuga, Fukuoka 816-8580, Japan*
[2]*Department of Interdisciplinary Studies, Faculty of Engineering, Tel Aviv University, Tel Aviv 69978, Israel*

We consider a two-dimensional (2D) model of a rotating attractive Bose-Einstein condensate (BEC), trapped in an external potential. First, a harmonic potential with the critical strength is considered, which generates quasisolitons at the lowest Landau level (LLL). We describe a family of the LLL quasisolitons using both numerical method and a variational approximation (VA), which are in good agreement with each other. We demonstrate that kicking the LLL mode or applying a ramp potential sets it in the Larmor (cyclotron) motion that can also be accurately modeled by the VA. Collisions between two such moving modes may be elastic or inelastic depending on their total norm. If an additional confining potential is applied along with the ramp, it creates a stationary edge state. Applying a kick to the edge state in the direction of the ramp gives rise to a skipping motion in the perpendicular direction. These regimes may be interpreted as the Hall effect for the quasisolitons. Next, we consider the condensate trapped in an axisymmetric quartic potential. Three species of localized states and their stability regions are identified, viz., vortices with arbitrary topological charge m, "crescents" (mixed-vorticity states), and strongly localized center-of-mass (c.m.) states, alias quasisolitons, shifted off the rotation pivot. These results are similar to those reported before for the model with a combined quadratic-quartic trap. Stable pairs of c.m. states set at diametrically opposite points are found, too. We present a VA which provides for an accurate description of vortices with all values of m, and of the c.m. states. We also demonstrate that kicking them in the azimuthal direction sets the quasisolitons in *epitrochoidal* motion (which is also accurately predicted by the VA), collisions between them being elastic.

I. INTRODUCTION

Formation of vortices is a well-known manifestation of superfluidity in Bose-Einstein condensates (BECs)—in particular, in those which form effectively two-dimensional ("pancake") configurations in appropriately designed trapping potentials [1]. If a condensate with repulsive interactions between atoms, which is confined in a nearly two-dimensional (2D) layer by a 2D harmonic (quadratic) potential with trapping frequency ω, is set in rotation with frequency Ω, formation of a multivortex lattice is observed in the experiment [2]. The stability of such lattices is limited to $\Omega < \omega$, as otherwise the centrifugal force empties the region in the center of the trap [3]. Close to the instability threshold, formation of a metastable state in the form of a giant vortex, with topological charge $m \sim 50$, was observed [4]. On the other hand, it was proposed theoretically [5] and implemented in the experiment [6] that the instability at $\Omega \geqslant \omega$ can be eliminated if the trapping potential is steeper than harmonic, the simplest possibility being to add a quartic term to it [in the critical case of $\Omega = \omega$, the linearized version of the respective 2D Gross-Pitaevskii equation (GPE) is tantamount to the Schrödinger equation for a charged particle in the uniform magnetic field, which gives rise to the Landau levels, see Eq. (6) below]. In many theoretical works, it has been demonstrated that self-repulsive condensates can form stable vortices with a multiple topological charge $m > 1$ in 2D anharmonic traps [7].

Dynamics of vortices in BEC with attraction between atoms is different—in particular, due to the possibility of the collapse in self-attractive media [8]. The stability of 2D vor-

tices confined by the harmonic potential was studied in detail [9]. It was demonstrated that, prior to the onset of the collapse, the vortex with $m = 1$ is destabilized by azimuthal perturbations that split it into mobile localized objects resembling fundamental solitons, if the norm of the vortex exceeds a certain critical value. Vortices with $m \geqslant 2$ are completely unstable in the same setting.

It was also predicted that, under the action of the rotation, BEC with the intrinsic attraction can break the 2D axial symmetry by self-trapping into quasisoliton objects, alias "center-of-mass" (c.m.) states, characterized by an offset of the c.m. from the rotation pivot [10]. It was concluded that the anharmonicity of the trapping potential is necessary for the stability of the c.m. states [11]. Therefore, the theoretical study of rotating attractive condensates trapped in quadratic-quartic radial potentials has drawn attention. Phase diagrams of this model were investigated in detail, both in the mean-field approximation (i.e., using the GPE and its linearization for small perturbations, in the form of the Bogoliubov-de Gennes equations) [12], and by means of a numerical diagonalization of the many-body bosonic Hamiltonian [13], both approaches producing similar results. Three types of stable localized patterns were identified in these studies: vortices with topological charge $m = 0, 1, 2, 3, \ldots$; crescent-shaped states with a broken axial symmetry, that may be realized, for instance, as a superposition of vortices with $m = 2, 3, 4$; and the c.m. states shifted from the rotation pivot. The transition between the crescents and c.m. states which feature stronger localization is gradual. It is also relevant to mention that crescents built similar to those reported in Refs. [11,12] can be made stable in a completely different model, viz., a quasilinear 2D equation with the harmonic trap whose strength

is proportional to the total norm of the configuration [14] (the so-called "accessible-soliton" model, which is relevant to nonlinear optics [15]).

The previous analysis of these states was carried out, in the framework of the GPE, in numerical form only. One of purposes of the present work is to demonstrate that the entire family of vortices, with all values of m, and the well-localized c.m. states can be predicted in an accurate form by a simple variational approximation (VA) (this method was applied to BEC in Ref. [16]; for a general review of variational techniques for solitons, see Ref. [17]). In addition, we find stable pairs of c.m. states set at diametrically opposite points. Another objective of this work is to consider the motion of c.m. states and collisions between them (which turn out to be elastic). The motion is also accurately described by the VA. To focus on effects of anharmonic traps, in that part of the work we consider the GPE with the quartic radial potential only, which may be implemented in the experiment [6].

Another setting considered in this work is the above-mentioned critical case of the quadratic axisymmetric trap with $\omega = \Omega$. In this case, we demonstrate that quasisolitons can be found in the lowest Landau level (LLL). Both quiescent and moving LLL modes are very accurately described by an appropriately modified VA. The motion of the Larmor (cyclotron) type is imposed on them by the application of a kick, or by the action of a 1D ramp potential. In addition, we consider the situation when the ramp acts in a combination with a 1D quartic potential. In the latter case, we find edge states of the nonlinear LLL modes, and also study their motion induced by the kick, which may be interpreted as an effective Hall effect for the quasisolitons. To the best of our knowledge, the Larmor motion and the drift motion are not reported before for the Bose-Einstein condensates. We hope that these types of analogs of Hall effect will be experimentally observed.

The paper is structured as follows. The underlying two-dimensional GPE and a brief description of the numerical method employed to look for stationary solutions (which is based on the integration in imaginary time) are presented in Sec. II. In Sec. III, we consider the quasisolitons of the LLL type in the critical model with the quadratic axisymmetric confining potential, while the model with the quartic potential is dealt with in Sec. IV. The paper is concluded in Sec. V.

II. THE MODEL AND NUMERICAL METHODS

The mean-field approximation for the 2D condensate trapped in potential $U(x,y)$ and rotating at angular velocity Ω is based on the GPE for the single-atom wave function, $\psi(x,y,t)$. In the scaled form, the equation, written in rotating coordinates x and y, takes the well-known form [10–12]

$$i\frac{\partial \psi}{\partial t} = \left[-\frac{1}{2}\left(\frac{\partial^2}{\partial x^2} + \frac{\partial^2}{\partial y^2}\right) - g|\psi|^2 + U(x,y) - \Omega \hat{L}_z \right]\psi. \quad (1)$$

Here $g \equiv -4\pi \mathcal{N} a_s/(M a_\perp) > 0$ is the effective self-attraction coefficient, with $\mathcal{N}$ the total number of atoms, $a_s < 0$ the scattering length of the attractive interatomic interactions, $a_\perp$ the transverse-trapping length, and $M = \iint |\psi(x,y)|^2 dxdy$

the norm of the 2D wave function, which is a dynamical invariant of Eq. (1). The orbital-momentum operator is $\hat{L}_z = i(y\partial_x - x\partial_y)$. In addition to M, Eq. (1) conserves the energy,

$$E = \int \left(\frac{1}{2}|\boldsymbol{\nabla}\psi|^2 - \frac{g}{2}|\psi|^4 + U|\psi|^2 - \Omega\psi^*\hat{L}_z\psi \right)d\mathbf{r}, \quad (2)$$

and the total angular momentum, $L = \int \psi^*\hat{L}_z\psi dr$, if the potential is axisymmetric, $U = U(r)$, with $r^2 \equiv x^2 + y^2$.

Steady-state solutions to Eq. (1) are looked for in the ordinary form, $\psi(x,y,t) = e^{-i\mu t}\phi(x,y)$, where μ is the real chemical potential, while stationary wave function $\phi(x,y)$ remains complex. To find configurations realizing a minimum of the energy, we used a modification of the known numerical method based on the integration of the GPE in imaginary time [18] (in Ref. [19], a similar method was used to generate vortex lattices in a 2D model with the repulsive nonlinearity and harmonic confining potential). To this end, we substitute real time t in Eq. (1) by $-i\tau$, introduce additional real variable $\widetilde{M}(\tau)$, and replace Eq. (1) by the following system of the Ginzburg-Landau (GL) type,

$$\frac{\partial \phi}{\partial \tau} = \left[\frac{1}{2}\nabla^2 + g|\phi|^2 - U(x,y) + \Omega\hat{L}_z + \gamma_1(\widetilde{M} - M) \right]\phi, \quad (3)$$

$$\frac{d\widetilde{M}}{d\tau} = \gamma_2(M_0 - M). \quad (4)$$

Here, M is the same 2D norm as defined above, but it is not a dynamical invariant of the GL equations, and M_0 is the target constant value of the norm in the stationary state to be found, while γ_1 and γ_2 are auxiliary positive constants.

Equation (4) acts as a negative feedback, which provides for the relaxation of the variable norm, $M(\tau)$, to M_0. Obviously, stationary states, into which solutions to Eqs. (3) and (4) relax at $\tau \to \infty$, also yield stationary solutions to GPE (1), with chemical potential $\mu = \gamma_1[\widetilde{M}(\tau \to \infty) - M_0]$.

Coupled equations (3) and (4) can be presented in the gradient form as

$$\frac{\partial \phi}{\partial \tau} = -\frac{\delta \widetilde{E}}{\delta \phi^*}, \quad \frac{d\widetilde{M}}{d\tau} = \frac{\gamma_2}{\gamma_1}\frac{\partial \widetilde{E}}{\partial \widetilde{M}}, \quad (5)$$

where $\widetilde{E} = E - (1/2)\gamma_1(\widetilde{M} - M_0)^2 + (1/2)\gamma_1(M - \widetilde{M})^2$. This representation demonstrates that Eqs. (3) and (4) may be regarded as equations generated by the minimization of functional E, under the constraint (Lagrangian condition) that the total norm is fixed, $M = M_0$. Fast convergence of numerical solutions of Eqs. (3) and (4) was achieved, for instance, with the choice of auxiliary parameters $\gamma_1 = 3$ and $\gamma_2 = 5$. On the other hand, if the convergence is achieved, the results do not depend on the choice of γ_1 and γ_2, which was verified by varying these constant in a broad range. The numerical integration was performed by means of the split-step 2D Fourier method with 256×256 modes.

We use Eq. (3) and Eq. (4) to obtain stationary solutions such as quasisolitons and vortices in several external potentials $U(x,y)$ in the following sections. The motion and the collision of the quasisolitons are simulated with the Gross-Pitaevskii equation (1).

III. LOWEST-LANDAU-LEVEL STATES

A. Quiescent modes

In the critical case when the confining potential is harmonic, with the respective frequency equal to the rotation velocity, $U = (1/2)\Omega r^2$, Eq. (1) and respective energy (2) reduce to

$$i\frac{\partial \psi}{\partial t} = \left[\frac{1}{2}\left(i\frac{\partial}{\partial x} - \Omega y\right)^2 + \frac{1}{2}\left(i\frac{\partial}{\partial y} + \Omega x\right)^2 - g|\psi|^2\right]\psi, \quad (6)$$

$$E = \int \left(\frac{1}{2}|(\boldsymbol{\nabla} - i\mathbf{A})\psi|^2 - \frac{g}{2}|\psi|^4\right)d\mathbf{r}, \quad (7)$$

where $\mathbf{A} = (-\Omega y, \Omega x)$. As said above, this system with $g = 0$ is equivalent to the 2D Schrödinger equation for a charged particle in uniform magnetic field Ω directed perpendicular to plane (x,y). The wave function of the corresponding ground state, i.e., the lowest Landau level (LLL), is

$$\psi = Ae^{-i\Omega t}\exp[-(\Omega/2)(x^2 + y^2)], \quad (8)$$

where A is an arbitrary amplitude.

For $g > 0$, a localized (quasisoliton) solution to nonlinear equation (6) may be approximated as an *ansatz* suggested by exact solution (8) for the linear equation,

$$\psi = Ae^{-i\mu t}\exp[-\alpha(x^2 + y^2)], \quad (9)$$

where A, α and μ are treated as variational parameters. Earlier, an ansatz using a product of the LLL wave function and an appropriate function in the perpendicular direction was used in Ref. [20] for the description of 3D vortices in rotating confined BECs.

The norm of ansatz (9) is

$$M = A^2\pi/(2\alpha). \quad (10)$$

Using this expression, we eliminate A in favor of M, and then calculate energy (7) corresponding to the ansatz,

$$E = M\left(\alpha + \frac{\Omega^2}{4\alpha} - \frac{gM\alpha}{2\pi}\right), \quad (11)$$

which does not contain μ. To predict the inverse-width parameter α of the localized state, we minimize the energy with respect to α, by setting $\partial E/\partial \alpha = 0$. This yields

$$\alpha = \frac{\Omega}{2}\frac{1}{\sqrt{1 - gM/(2\pi)}}. \quad (12)$$

Then, the substitution of this result into Eq. (10) yields the respective expression for the amplitude,

$$A^2 = \frac{\Omega M}{\pi\sqrt{1 - gM/(2\pi)}}. \quad (13)$$
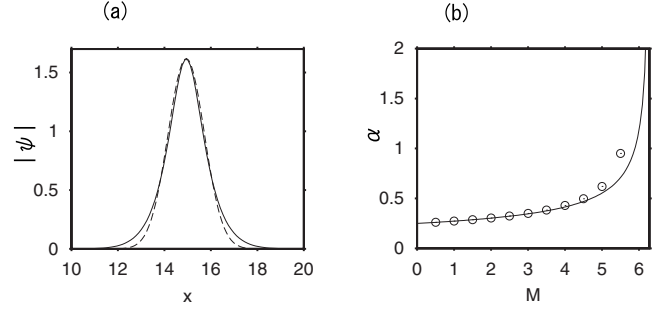
The energy is calculated as

FIG. 1. (a) A typical shape of the nonlinear localized mode supported by the LLL (lowest Landau level) for $M = 5$. (b) Comparison of the numerically found inverse-width parameter α with the approximation provided by the variational method. Other parameters in this figure are $g = 1$ and $\Omega = 0.5$.

$$E = M\left(\frac{\Omega}{2\sqrt{1 - gM/(2\pi)}} + \frac{\Omega\sqrt{1 - gM/(2\pi)}}{2}\right.$$
$$\left. - \frac{gM\Omega}{4\pi\sqrt{1 - gM/(2\pi)}}\right), \quad (14)$$

which is approximated as $E \sim M[\Omega - gM\Omega/(4\pi)]$ near $g = 0$. Note that expression (13) diverges at $gM = 2\pi$, which implies the collapse in the 2D setting due to the self-attraction. This collapse threshold is a well-known prediction of the VA [21], which does not depend on the presence of the external potential or rotation.

Figure 1(a) displays a numerically found profile of the central cross section of $\psi(x,y)$ for $g = 1$ and $M = 5$. The dashed curve in the same figure is the Gaussian fitting to the numerical profile, $\psi_{\mathrm{fit}}(x,y) = A_{\mathrm{fit}}\exp[-\alpha_{\mathrm{fit}}(x - L/2)^2]$, with $A_{\mathrm{fit}} = 1.62$ and $\alpha_{\mathrm{fit}} = 0.824$. Note that the central part of the 2D mode is slightly narrower than the Gaussian, because M is rather large, inducing self-compression of the mode. The solid curve in Fig. 1(b) displays the prediction of the VA for inverse-width parameter α, given by Eq. (12), while the chain of circles represent numerical values of the same parameter, which were found from an integral expression, $M/[2\iint(x^2 + y^2)|\psi(x,y)|^2 dxdy]$. Indeed, if ansatz (9) is substituted into this expression, it will yield exactly α.

Modes with the intrinsic angular momentum, i.e., localized vortices, can also be constructed in this setting. An ansatz for the localized vortex is

$$\psi = Ae^{-i\mu t}(x + iy)\exp[-\alpha(x^2 + y^2)]. \quad (15)$$

The norm of ansatz (15) is $M = \pi A^2/(4\alpha^2)$ and the energy E is given by

$$E = M\left(2\alpha - \Omega + \frac{\Omega^2}{2\alpha} - \frac{gM\alpha}{4\pi}\right). \quad (16)$$

The inverse-width parameter α is similarly obtained by the minimization of the energy as
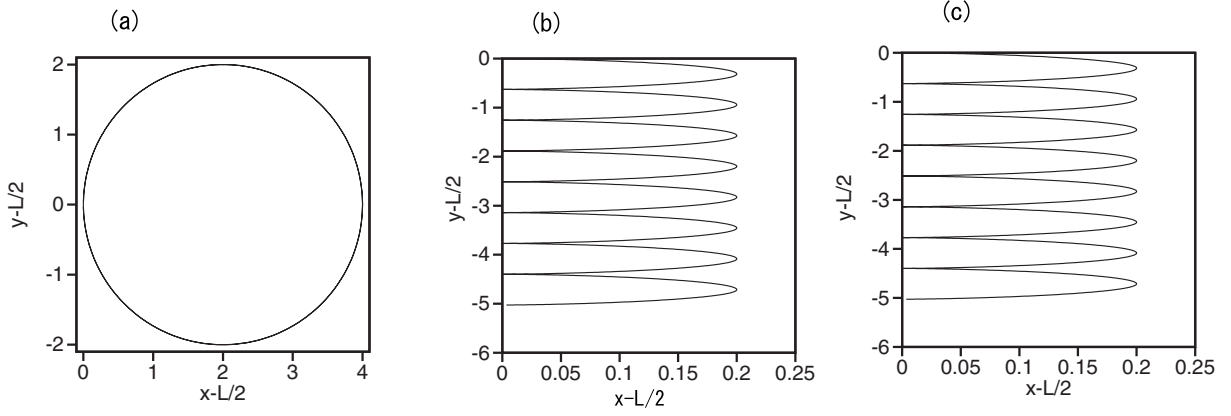
FIG. 2. (a) The Larmor motion of the c.m. of the LLL quasisoliton initiated by the application of kick $k_y=2$ in the y direction, for $g=1$ and $M=5$. (b) The drift of the c.m. in the ramp potential, $U_{\text{extra}}=-0.1x$, again for $g=1$ and $M=5$. (c) The drift of the c.m. under the action of the same tilted potential, but for for $g=0$ (in the linear Schrödinger equation).

$$\alpha = \frac{\Omega}{2} \frac{1}{\sqrt{1 - gM/(4\pi)}}. \tag{17}$$

The inverse-width parameter α is equal to $\Omega/2$ at $g=0$, and the divergence occurs at $gM=4\pi$. The energy E is calculated as

$$E = M\left(\frac{\Omega}{\sqrt{1 - gM/(4\pi)}} - \Omega + \Omega\sqrt{1 - gM/(4\pi)} \right.$$
$$\left. - \frac{gM\Omega}{8\pi\sqrt{1 - gM/(4\pi)}} \right), \tag{18}$$

which is approximated as $E \sim M[\Omega - gM\Omega/(8\pi)]$ near $g=0$. The vortex and the quasisoliton have the same energy at $g=0$. The quasisoliton has a lower energy in the case of attractive interaction $g>0$ than the localized vortex, however, the energy of the localized vortex is lower that the quasisoliton in the case of the repulsive interaction $g<0$. This is a reason why vortex states appear in the case of repulsive interaction. The Gaussian type wave function ψ was numerically obtained near the lowest-Landau-level regime in the previous paper [19].

B. The Larmor motion

If the localized state placed at $(x_0,y_0)=(0,0)$ is kicked by lending it wave number k_y in the y direction, $\psi(x,y) \to \psi(x,y)\exp(ik_y y)$, the quasisoliton exhibits rotating Larmor (cyclotron) motion, as shown in Fig. 2(a). If a ramp (constant external force) is applied in the x direction, by adding the extra potential term, $U_{\text{extra}}(x)=-Fx$, to energy (7), the quasisoliton becomes engaged in a drift motion, as shown in Fig. 2(b). These scenarios of the Larmor motion of the quasisoliton are qualitatively the same as exhibited by the LLL localized state in the limit of the linear Schrödinger equation ($g=0$), as shown in Fig. 2(c). One can check, by means of direct simulations, that a localized vortex with vorticity $m=1$ also exhibits the Larmor motion in the same linear Schrödinger equation.

The Larmor motion induced by the additional potential can also be explained via the variational method. The La-grangian corresponding to Eq. (6), with the addition of the extra potential, is

$$L = \int \left(\frac{i}{2}(\psi_t\psi^* - \psi_t^*\psi) - \frac{1}{2}|(\nabla - i\mathbf{A})\psi|^2 \right.$$
$$\left. + \frac{g}{2}|\psi|^4 - U_{\text{extra}}(x,y)|\psi|^2 \right)d\mathbf{r}. \tag{19}$$

If $\psi(x,y,t)$ is approximated by a generalization of ansatz (9), viz.,

$$\psi = Ae^{-i\mu t}\exp(-\alpha\{[x-x_0(t)]^2 + [y-y_0(t)]^2\})$$
$$\times\exp\{ip_x[x-x_0(t)] + ip_y[y-y_0(t)]\}, \tag{20}$$

the corresponding effective Lagrangian takes the following form, after a straightforward calculation,

$$\frac{L_{\text{eff}}}{M} = p_x\dot{x}_0 + p_y\dot{y}_0 - \alpha - \frac{\Omega^2}{2}(x_0^2 + y_0^2) - \frac{1}{2}(p_x^2 + p_y^2) - \frac{1}{4\alpha}\Omega^2$$
$$+ \frac{gM\alpha}{2\pi} - \Omega(p_xy_0 - p_yx_0) - U_{\text{eff}}(x_0,y_0), \tag{21}$$

where the overdot stands for the time derivative, and

$$U_{\text{eff}}(x_0,y_0,\alpha) \equiv \frac{A^2}{M}\int\int U_{\text{extra}}(x,y)\exp(-\alpha\{[x-x_0(t)]^2$$
$$+ [y-y_0(t)]^2\})dxdy. \tag{22}$$

The system of the Euler-Lagrange variational equations is then derived from the effective Lagrangian,

$$\frac{dp_x}{dt} = \Omega p_y - \frac{\partial U_{\text{eff}}}{\partial x_0},$$

$$\frac{dp_y}{dt} = -\Omega p_x - \frac{\partial U_{\text{eff}}}{\partial y_0},$$
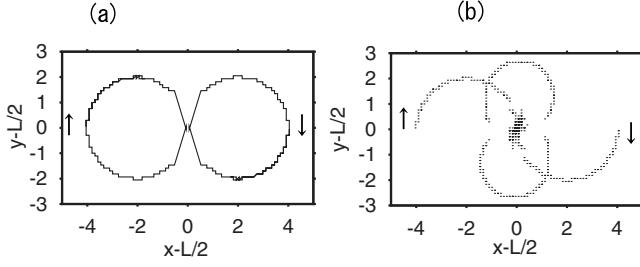
$$\frac{dx_0}{dt} = p_x + \Omega y_0,$$

FIG. 3. (a) Trajectories of points of maxima of $|\psi(x,y)|$ in half planes $x>L/2$ and $x<L/2$ for a pair of LLL quasisolitons with norm $M=1$, kicked by $k_y=\pm 2$. The solitons survive multiple elastic solutions. The arrows shows the initial positions and velocities of the two solitons. (b) The same for $M=5$. In this case, the collision results in the fusion and collapse of the LLL quasisolitons.

$$\frac{dy_0}{dt} = p_y - \Omega x_0,$$

$$-1 + \frac{gM}{2\pi} + \frac{\Omega^2}{4\alpha^2} - \frac{\partial U_{\text{eff}}}{\partial \alpha} = 0. \quad (23)$$

In the simplest case of the uniform ramp, corresponding to $U_{\text{extra}}=-Fx$, i.e., $\partial U_{\text{eff}}/\partial\alpha=0$, the last equation in system (23) yields the same constant expression for α as given above by Eq. (12). With constant α (i.e., constant width of the LLL mode), the remaining part of system (23) amounts to coupled equations of motion of the second order,

$$\frac{d^2 x_0}{dt^2} = 2\Omega \frac{dy_0}{dt} - \frac{\partial U_{\text{eff}}}{\partial x_0},$$

$$\frac{d^2 y_0}{dt^2} = -2\Omega \frac{dx_0}{dt} - \frac{\partial U_{\text{eff}}}{\partial y_0}. \quad (24)$$

With $U_{\text{eff}}=0$, this system describes the Larmor (cyclotron) motion, and for $U_{\text{eff}}=-Fx_0$, Eqs. (24) predict an overlap of the Larmor rotation and drift in the y direction. The drift motion, in the direction perpendicular to the ramp, is an analog of the ordinary Hall effect in solid-state physics (similarities between the soliton dynamics in BEC and the quantum Hall effect were discussed in various contexts, see, e.g., Ref. [22] and references therein). Additional analogies to the Hall effect are considered below.

If two LLL quasisolitons are kicked in opposite directions, by imparting wave numbers $\pm k_y$ to them, the Larmor motion of the solitons eventually results in a collision. If the norm of each quasisoliton is not too large, the collision seems completely elastic, and the two objects keep moving in closed trajectories which together form a "figure of eight," surviving multiple collisions, as shown in Fig. 3(a) for $M=1$, $g=1$, and $k_y=2$. On the other hand, if the norm of each LLL mode is larger, the collision is inelastic, reducing the wave numbers of the quasisolitons, and thus making the radius of the Larmor motion smaller. This case is illustrated by Fig. 3(b) for $M=5$. Inelastic collisions between 2D solitons which are too "heavy" and can also suffer the merger and collapse were reported in different settings, such as quasi-1D guiding channels [23].

C. The Hall effect and edge states for the quasisolitons

As mentioned above, the analog of the Hall effect for matter-wave solitons is a subject of considerable interest [22]. To study it in the present context, i.e., as a matter of fact, to consider the corresponding *edge states* of the LLL quasisolitons, we combine the ramp with a weak holding quartic potential in the x direction, by taking $U_{\text{extra}}=-Fx+bx^4$, with small $b>0$. Here, the edge state is a state which represents the Hall effect near the sample edge [24]. Usually a sharp potential wall is assumed to confine an electron inside of the sample, but we have used a quartic potential in this section because it is a milder potential and the variational method is more easily applied, and the model is closely related to the axisymmetric quartic model discussed in the next section.

The VA can be used in this setting too. To this end, we approximate ψ by an anisotropic Gaussian ansatz,

$$\psi = Ae^{-i\mu t}\exp[-\alpha(x-x_0)^2 - \beta(y-y_0)^2]\exp\{ip_x[x-x_0(t)] + ip_y[y-y_0(t)]\}, \quad (25)$$

cf. expression (20). The substitution of ansatz (25) in Lagrangian (19) yields

$$\frac{L_{\text{eff}}}{M} = p_x\dot{x}_0 + p_y\dot{y}_0 - \frac{1}{2}(\alpha+\beta) - \frac{\Omega^2}{2}(x_0^2+y_0^2) - \frac{1}{2}(p_x^2+p_y^2)$$

$$- \frac{\Omega^2}{8}\left(\frac{1}{\alpha}+\frac{1}{\beta}\right) + \frac{gM}{2\pi}\sqrt{\alpha\beta} - \Omega(p_xy_0-p_yx_0)$$

$$- U_{\text{eff}}(x_0,y_0), \quad (26)$$

where, this time, the norm is $M=A^2\pi/(2\sqrt{\alpha\beta})$, and

$$U_{\text{eff}}(x_0,y_0) = -Fx_0 + b(x_0^2+y_0^2)^2$$

$$+ \frac{b}{2\alpha}(3x_0^2+y_0^2) + \frac{b}{2\beta}(x_0^2+3y_0^2), \quad (27)$$

cf. Eqs. (21) and (22). The respective equations of motion are written as

$$\frac{d^2 x_0}{dt^2} = 2\Omega \frac{dy_0}{dt} - \frac{\partial U_{\text{eff}}}{\partial x_0},$$

$$\frac{d^2 y_0}{dt^2} = -2\Omega \frac{dx_0}{dt} - \frac{\partial U_{\text{eff}}}{\partial y_0},$$

$$-\frac{1}{2} + \frac{gM}{4\pi}\sqrt{\frac{\beta}{\alpha}} + \frac{\Omega^2}{8\alpha^2} - \frac{\partial U_{\text{eff}}}{\partial\alpha} = 0,$$

$$-\frac{1}{2} + \frac{gM}{4\pi}\sqrt{\frac{\alpha}{\beta}} + \frac{\Omega^2}{8\beta^2} - \frac{\partial U_{\text{eff}}}{\partial\beta} = 0. \quad (28)$$

Stationary solutions to Eqs. (28) are determined by algebraic relations

$$\dot{y}_0 = 0, \quad 4bx_0^3 + b(3/\alpha+1/\beta)x_0 = F, \quad (29)$$

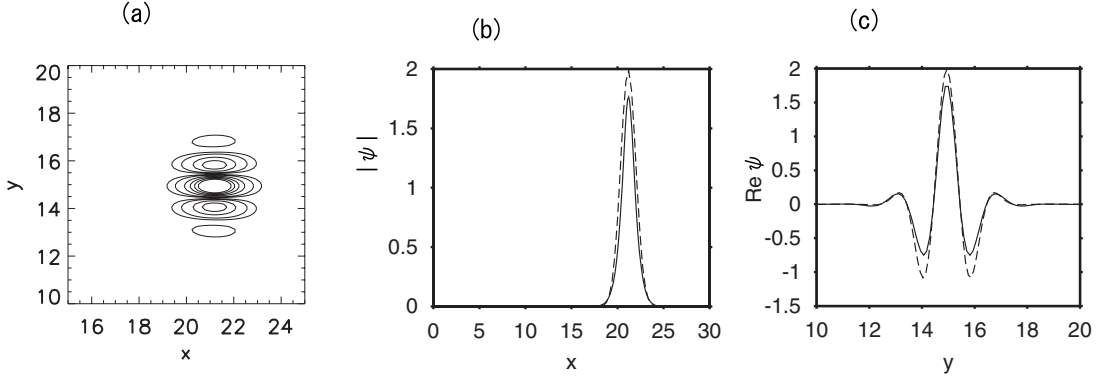$$-(1/2) + gM/(4\pi)\sqrt{\beta/\alpha} + \Omega^2/(8\alpha^2) + 3bx_0^2/(2\alpha^2) = 0, \quad (30)$$

FIG. 4. (a) The contour plot of $\text{Re}[\psi(x,y)]$ of the edge state, for $g=1$, $M=5$, $F=0.5$, and $b=0.0005$. (b) The profile of $|\psi(x,y)|$ at $y=L/2$. (c) $\text{Re}\{\psi(x,y)\}$ at $x=21.2$. The two latter panels include comparison with profiles predicted by the variational approximation.

$$-(1/2) + gM/(4\pi)\sqrt{\alpha/\beta} + \Omega^2/(8\beta^2) + bx_0^2/(2\beta^2) = 0. \tag{31}$$

In the linear limit $(g=0)$, these relations yield $\alpha = \sqrt{\Omega^2/4 + 3bx_0^2}$ and $\beta = \sqrt{\Omega^2/4 + bx_0^2}$, with the wave number in the y direction being $p_y = \Omega x_0 > 0$.

As an example, we refer to the LLL mode in the edge state that was found in the numerical form for $M=5$, $F=0.5$, $b=0.0005$, $g=1$, and $\Omega=0.5$. Fitting this mode to Gaussian ansatz (25), the corresponding parameters were numerically evaluated as $x_0=6.225$, $\alpha=0.724$, $\beta=0.679$, $A \equiv (4\alpha\beta/\pi)^{1/4}\sqrt{M}=1.99$, and $p_y=\Omega x_0$. Figures 4(a) and 4(b) display, respectively, the contour plot of $\text{Re}[\psi(x,y)]$ and cross-section profile $|\psi(x,y)|$ at $y=L/2$, which is compared to its counterpart predicted by the VA through Eqs. (25) and (30). In addition, Fig. 4(c) displays $\text{Re}[\psi(x,y)]$ at $x=21.2$, which is compared to the respective approximation provided by ansatz (25), $A\exp[-\beta(y-L/2)^2]\cos(p_yy)$.

If the edge state is kicked with wave number k_y, the quasisoliton exhibits drift motion. For parameters identical to those in Fig. 4, in Fig. 5 we display the trajectory of its c.m., initiated by the kick with $k_y=1$, and the same trajectory as
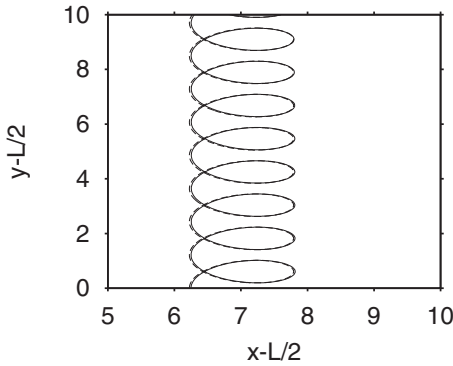

FIG. 5. The trajectory of the drift motion of an edge LLL mode, kicked with $k_y=1$, for $g=1$, $F=0.5$, $b=0.0005$, and $M=5$, as obtained from direct numerical simulations of the GPE (the solid curve), and the counterpart of the same trajectory, predicted by the variational approximation (the dashed curve).

predicted by variational equations (28). These results demonstrate that the VA provides quite a reasonable accuracy for the description of dynamical states, as well as for static ones.

IV. THE AXISYMMETRIC QUARTIC POTENTIAL

In the rest of the paper, we focus on a different situation, namely, the setting with the quartic axisymmetric potential $U(x,y)=br^4$, where b is a small positive constant. The purpose of the consideration of this model is to highlight the dynamics on vortices and quasisolitons under the anharmonic confinement. The confinement potential is not a critical harmonic potential $U=(1/2)\Omega r^2$ assumed in the previous section, and the system is deviated from the lowest-Landau-level regime. The respective variant of the GPE is [cf. Eq. (6)]

$$i\frac{\partial\psi}{\partial\tau} = \left(-\frac{1}{2}\nabla^2 - \Omega\hat{L}_z - g|\phi|^2 + br^4\right)\phi, \tag{32}$$

where ∇^2 is the 2D Laplacian, and the angular-momentum operator is $\hat{L}_z = i(x\partial_y - y\partial_x)$.

Similar to Eqs. (3) and (4), steady-state solutions to Eq. (1) are looked for through the simulations of relaxation in the following modified system of the GL type:

$$\frac{\partial\phi}{\partial\tau} = \left(\frac{1}{2}\nabla^2 + g|\phi|^2 - br^4 + \Omega\hat{L}_z + \gamma_1(\tilde{M}-M)\right)\phi, \tag{33}$$

$$\frac{d\tilde{M}}{d\tau} = \gamma_2(M_0 - M). \tag{34}$$

Here, M is the same 2D norm as defined above, and M_0 is the target constant value of the norm in the stationary state to be found.

Using the remaining scaling invariance of Eq. (1), we fix normalizations by choosing $b=0.002$ (a small value of trapping coefficient b is necessary to allow the condensate enough room to evolve), and $M_0=4$. Axisymmetric vortex solutions to Eqs. (33) and (34) with topological charge m are sought for as $\phi=r^m e^{im\theta}R_m(r,\tau)$, where the reduced amplitude function R_m satisfies the following equations:
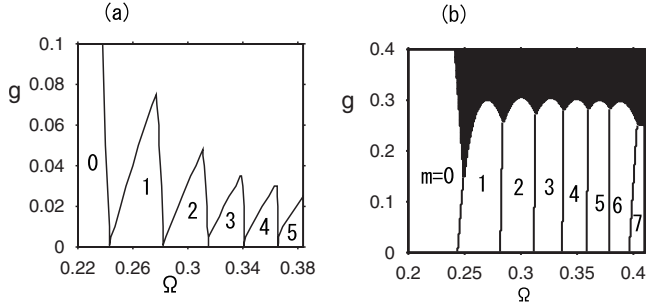
FIG. 6. (a) The numerically generated stability diagram for vortices with different values of topological charge m, in the plane of the rotation frequency and strength of the attractive interaction, Ω and g, in the model with the quartic confining potential. (b) Regions where the variational approximation predicts that vortices with charge m or c.m. states, alias quasisolitons (the black area), provide for a minimum of the energy.

$$\frac{\partial R_m}{\partial \tau} = \frac{1}{2}\left(\frac{\partial^2}{\partial r^2} + \frac{2m+1}{r}\frac{\partial}{\partial r} - 2br^4\right)R_m + gr^{2m}R_m^3 + m\Omega R_m$$

$$+ \alpha(\widetilde{M} - M)R_m, \tag{35}$$

$$\frac{d\widetilde{M}}{d\tau} = \beta(M_0 - M), \quad M(\tau) = 2\pi\int_0^\infty r^{2m+1}R_m^2 dr. \tag{36}$$

Once stationary solutions were found, their stability was examined by means of computation of the respective eigenvalues, using the Bogoliubov-de Gennes equations, i.e., the linearization of Eq. (1), for small perturbations built (for given m) as superpositions of components with vorticities $m \pm 1$ (such perturbation modes turn out to be most dangerous in terms of the instability).

The results, in the form of a stability diagram in the plane of (Ω, g) for $m=0,1,2,3,4,5$, are presented in Fig. 6(a). Each stability domain for $m \geqslant 1$ is bounded by two curves, which are generated by critical perturbation eigenmodes that are found to be, respectively, real and imaginary, with respect to unperturbed amplitude functions $R_m(r)$. This stability diagram is qualitatively similar to those reported in the model with a mixed quadratic-quartic radial trap [12,13]. For given $\Omega > 0$, vortices with $m < 0$ can be found, too, but they all are unstable. This instability can be readily explained by the fact that the Coriolis term in the vortex' energy, which is proportional to $-m\Omega$, is positive for $m < 0$, see Eq. (38) below.

While the increase of Ω at fixed self-attraction coefficient g leads to the transition to vortices with larger m, the vortex states become unstable with the increase of g, being replaced by crescent-shaped ones, as shown in Fig. 7. In Refs. [12,14], similar patterns were interpreted (in models with the local and nonlocal nonlinearity, respectively) as superpositions of vortices with three different values of the topological charge, viz., given m and $m \pm 1$. This fact agrees with the above-mentioned finding that perturbation modes which can destabilize a given vortex carry vorticities $m \pm 1$. Further increase of g leads to a reduction of the crescent's length and its gradual compression into a strongly localized c.m. state, alias quasisoliton, which carries an intrinsic phase gradient along the azimuthal direction, see Fig. 7(c); note that the value of g corresponding to the quasisoliton falls below the collapse threshold. The shift of the c.m. state from the rotation pivot increases with Ω. This quasisoliton is similar to the edge state of the LLL type shown above in Fig. 4.

In the limit of large m, the stationary version of Eqs. (35) and (36) give rise to a simple *asymptotically exact* solution, which does not depend on g and b,

$$R_m(r) = \sqrt{M_0\Omega^{m+1}/(\pi m!)}\exp(-\Omega r^2/2) \tag{37}$$

(recall we here fix the norm as $M_0=4$). This solution, and numerical results obtained for finite m, suggest to approximate the stationary solution for vortices by ansatz $\phi = Ae^{im\theta}r^m\exp(-\alpha r^2)$, whose norm is $M_0 = \pi m!(2\alpha)^{-(m+1)}A^2$. The substitution of the ansatz in Eq. (2) yields the corresponding expression for the energy,

$$\frac{E}{M_0} = -m\Omega + \frac{(m+2)(m+1)b}{4\alpha^2} + \alpha(m+1)$$

$$- (2m)!M_0 g\alpha/[2^{2m+1}(m!)^2\pi]. \tag{38}$$

Then, width parameter α for the solution sought for is determined by the minimization of the energy, $\partial E/\partial\alpha = 0$, which yields

$$\alpha^{-3} = \frac{2}{b(m+2)(m+1)}\left(m + 1 - \frac{(2m)!M_0 g}{2^{2m+1}(m!)^2\pi}\right). \tag{39}$$

On the other hand, a quasisoliton with the c.m. located at distance x_0 from the pivot, see Fig. 7(c), may be approximated by the anisotropic ansatz, which is similar to the one used above in Eq. (25),
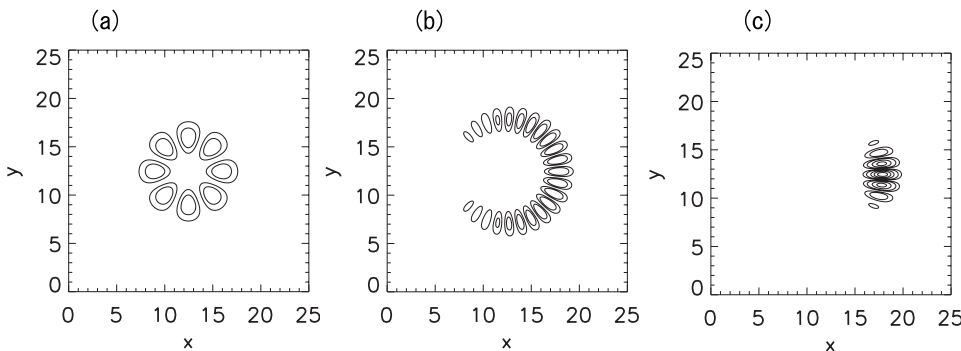

FIG. 7. Generic examples of stable matter-wave patterns in the rotating condensate confined by the quartic potential are shown by means of contour plots of $|\text{Re}[\phi(x,y)]|$: (a) a vortex with $m=4$, for $g=0.01$, $\Omega=0.35$; (b) a crescent, for $g=0.001$, $\Omega=0.5$; (c) a strongly compressed c.m. state (quasisoliton), for $g=0.5$, $\Omega=0.5$.
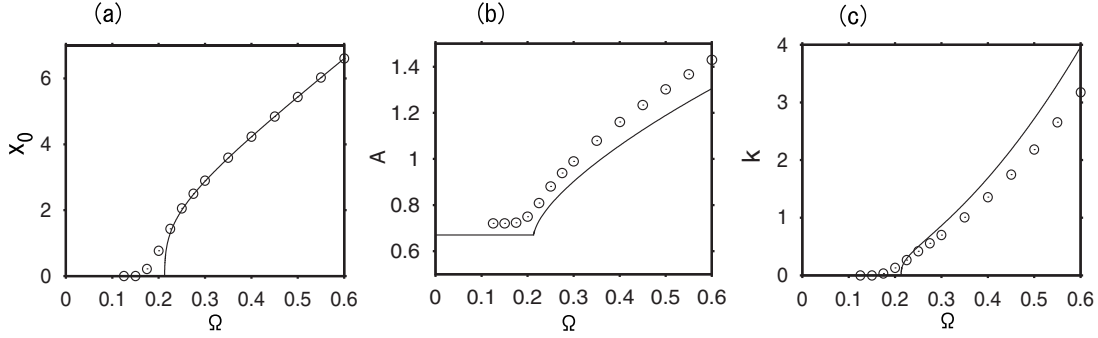
FIG. 8. Parameters of stable quasisolitons trapped in the quartic axisymmetric potential, as found from the numerical computations (circles) and predicted by the variational approximation (curves) for $g=1$: (a) the shift from the rotation pivot; (b) amplitude; (c) intrinsic wave number.

$$\psi = A\exp\{iky - [\alpha(x-x_0)^2 + \beta y^2]\}, \qquad (40)$$

with norm $M_0 = \pi A^2/(2\sqrt{\alpha\beta})$. If this c.m. state was generated by an unstable vortex with charge m, comparison of the azimuthal phase gradients suggests that $k = m/x_0$. When substituted in Eq. (2), ansatz (40) yields

$$\frac{E}{M_0} = \frac{\alpha + \beta + k^2}{2} - \Omega k x_0 - \frac{g\sqrt{\alpha\beta}M_0}{2\pi}$$
$$+ \frac{b[3\beta^2 + 2\alpha\beta(1 + 12\beta x_0^2) + \alpha^2(3 + 8\beta x_0^2 + 16\beta^2 x_0^4)]}{16\alpha^2\beta^2}.$$
$$(41)$$

Values of the variational parameters are predicted by equations $\partial E/\partial x_0 = \partial E/\partial k = \partial E/\partial \alpha = \partial E/\partial \beta = 0$, which yield, in particular,

$$k = \Omega x_0, \quad x_0^2 = [\Omega^2\alpha\beta - b(3\beta + \alpha)]/(4b\alpha\beta), \qquad (42)$$

if $x_0 \neq 0$. Another solution, with $x_0 = 0$ (an isotropic soliton sitting at the center, which is stable for small Ω) has $k = 0$ and $\alpha = \beta = [(2\pi b)/(2\pi - M_0)]^{1/3}$. Further analysis of the VA solutions (without fixing $M_0 = 4$) demonstrates that they predict the collapse (nonexistence of solutions) at $M_0 \geq 2\pi$, in accordance with the known variational result [21].

Using the VA solutions and expressions (38) and (41), we have identified, as shown in Fig. 6(b), regions in parameter plane (Ω, g) where vortices with particular integer values of m, or the c.m. state provide for the minimum of the energy, i.e., determine the ground state. Comparison with the numerically identified stability regions for vortices in Fig. 6(a) demonstrates that the VA predicts transitions between different values of m with the increase of Ω quite accurately. The discrepancy in Fig. 6 between the numerical and variational plots in the direction of g has an obvious reason: the VA does not take into regard the other species of the localized states, viz., crescents, alias mixed-vorticity states [see Fig. 7(b)]. In fact, crescents have their own domain of the energy dominance, between those of the vortices and c.m. states. Note that solution (37), which is asymptotically exact for $m \to \infty$, and expression (38) predict the equality between energies of vortices with m and $m+1$, i.e., borders between the energy-dominance areas of these states (for $g \to 0$), at $\Omega_m \approx (4bm)^{1/3}$. To directly test the accuracy of the VA, in Fig. 8

we display a comparison between characteristics of the quasisolitons, viz., c.m. offset x_0, amplitude A, and wave number k, as found from numerical results and predicted by the VA.

The variational results presented above suggest that the model may also support a pair of c.m. states placed at diametrically opposite points. Indeed, Eq. (42) gives rise to two roots, $x_0 = \pm\sqrt{[\Omega^2\alpha\beta - b(3\beta + \alpha)]/(4b\alpha\beta)}$, which correspond to opposite values of y wave number k. Such *stable* quasisoliton pairs can be readily found from the numerical solution, see a typical example in Fig. 9. In the experiment, the pair can be created, for instance, by originally adding a strong blue-detuned (repulsive) light sheet which cuts the circular trap into semicircles. After two c.m. states have self-trapped, the sheet may be turned off, to restore the axial symmetry of the trap.

V. THE MOTION AND COLLISIONS OF QUASISOLITONS

Although they were obtained above as quiescent solutions, the localized c.m. states can be readily set in motion by the application of tangential kick $\exp(iqy)$ with wave number q, similar to how this was done above for the LLL localized modes. As a result, the quasisoliton exhibits rotary motion, following a trajectory in the form of an *epitrochoid*, see a typical example in Fig. 10.
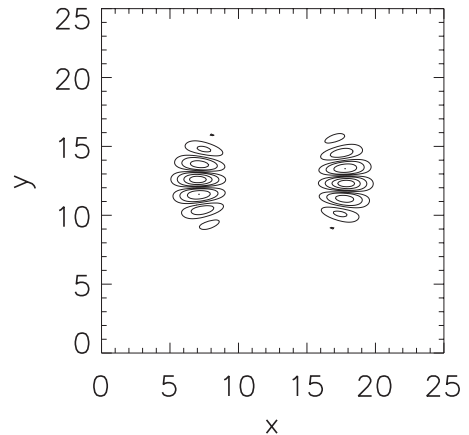

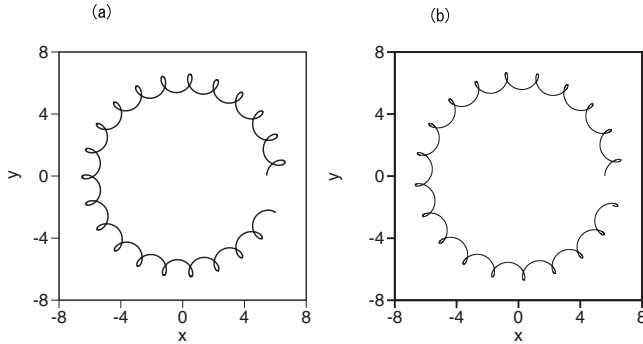FIG. 9. A generic example of a stable pair of two strongly compressed c.m. states found for $g=0.5$, $\Omega=0.5$.

FIG. 10. (a) The trajectory of the c.m. motion of a quasisoliton kicked with wave number $q=1$, for $g=1$, $\Omega=0.5$, in the model with the quartic axisymmetric trap. (b) Its counterpart predicted by the variational approximation.

Following the approach elaborated above for the moving LLL modes, we present a similar analytical description of the kicked quasisoliton in the model with the quartic confinement. To this end, we adopt the same ansatz (20) as used above, and use the Lagrangian corresponding to Eq. (32),

$$L = \int \left(\frac{i}{2}(\psi_t \psi^* - \psi_t^* \psi) - \frac{1}{2}|\nabla \psi|^2 + \Omega \psi^* \hat{L}_z \psi + \frac{g}{2}|\psi|^4 - br^4|\psi|^2 \right) d\mathbf{r},$$ (43)

cf. Eq. (19). The substitution of the ansatz in this Lagrangian and straightforward calculations lead to the following equations of motion for the c.m. mode:

$$\frac{d^2 x_0}{dt^2} = 2\Omega \frac{dy_0}{dt} - \frac{\partial U_{\text{eff}}}{\partial x_0},$$

$$\frac{d^2 y_0}{dt^2} = -2\Omega \frac{dx_0}{dt} - \frac{\partial U_{\text{eff}}}{\partial y_0},$$ (44)

with $U_{\text{eff}}(r) = -(1/2)\Omega^2 r^2 + br^4 + (2b/\alpha)r^2$. Figure 10(b) displays a counterpart of the numerically found trajectory from Fig. 10(a), as produced by Eqs. (44) for $g=1$, $b=0.002$, and $\alpha=0.532$. The initial velocity is $dx_0/dt=0$, $dy_0/dt=1$. It is seen that the VA matches the numerical findings very well in this case, too.

The possibility of the motion of the c.m. states suggests to consider collisions between them, also in analogy with what was done above for the LLL modes. In Fig. 11, we display a typical example of the collision, which is generated by applying kicks with $q=\pm 0.5$ to identical quasisolitons with their c.m. placed, originally, at diametrically opposite points (in the experiment, such an initial configuration can be created as outlined at the end of the previous section). The
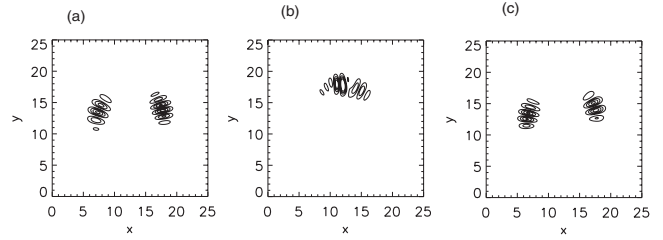

FIG. 11. Snapshots of $|\text{Re}\{\psi(x,y,t)\}|$, at (a) $t=10$, (b) $t=50$, and (c) $t=90$ illustrating an elastic collision between counter-rotating c.m. states kicked by $q=\pm 0.5$, at $g=0.5$, $\Omega=0.5$.

kicked solitons are no longer identical because term $\Omega \hat{L}_z$ in Eq. (32) breaks the symmetry between the clockwise and counterclockwise directions of the rotation. Nevertheless, the collisions are elastic, with the quasisolitons recovering their shapes after the collision.

VI. CONCLUSION

We have revisited the 2D model of rotating BEC with attraction between atoms. Two different situations of special physical interest were considered: the one with the critical strength of the quadratic confining potential, and the purely quartic axisymmetric trap. In the former case, the linear limit of the GPE (Gross-Pitaevskii equation) is tantamount to the Schrödinger equation for a charged particle moving in the uniform magnetic field. We have demonstrated that the action of the self-focusing nonlinearity on the localized state corresponding to the wave function at the LLL (lowest Landau level) gives rise to stable quasisolitons. These states, both quiescent ones and those set in motion by the kick, or under the action of the ramp potential, are very accurately described by the VA (variational approximation). We have also considered the situation when an external weak 1D quartic potential acts in combination with the ramp, which gives rise to edge states emulating the Hall effect in terms of the matter-wave quasisolitons.

In the case when the axisymmetric trap is represented by the quartic potential, we have developed the VA which provides for an accurate description of two species of stable localized states in the model, namely, vortices with an arbitrary value of the topological charge, and c.m. modes shifted off the rotation pivot, alias quasisolitons. Stable states in the form of two c.m. modes placed at diametrically opposite sites were found too. The other species, crescents, was obtained in the numerical form. It was also demonstrated that kicking the c.m. state in the tangential direction sets it in motion along an *epitrochoidal* trajectory, and collisions between such solitons are elastic. The motion of the kicked quasisoliton in the latter situation is also accurately predicted by the VA.

[1] C. J. Pethick and H. Smith, *Bose-Einstein Condensation in Dilute Gases* (Cambridge University Press, Cambridge, 2002).

[2] J. R. Abo-Shaeer, C. Raman, J. M. Vogels, and W. Ketterle, Science **292**, 476 (2001).

[3] P. Rosenbusch, D. S. Petrov, S. Sinha, F. Chevy, V. Bretin, Y. Castin, G. Shlyapnikov, and J. Dalibard, Phys. Rev. Lett. **88**, 250403 (2002).

[4] P. Engels, I. Coddington, P. C. Haljan, V. Schweikhard, and E. A. Cornell, Phys. Rev. Lett. **90**, 170405 (2003).

[5] E. Lundh, Phys. Rev. A **65**, 043604 (2002).

[6] V. Bretin, S. Stock, Y. Seurin, and J. Dalibard, Phys. Rev. Lett. **92**, 050403 (2004).

[7] A. L. Fetter, Phys. Rev. A **64**, 063608 (2001); E. Lundh, *ibid.* **65**, 043604 (2002); K. Kasamatsu, M. Tsubota, and M. Ueda, *ibid.* **66**, 053606 (2002); G. M. Kavoulakis and G. Baym, New J. Phys. **5**, 51 (2003); A. Aftalion and I. Danaila, Phys. Rev. A **69**, 033608 (2004); U. R. Fischer and G. Baym, Phys. Rev. Lett. **90**, 140402 (2003); A. D. Jackson and G. M. Kavoulakis, Phys. Rev. A **70**, 023601 (2004); T. K. Ghosh, *ibid.* **69**, 043606 (2004).

[8] G. Baym and C. J. Pethick, Phys. Rev. Lett. **76**, 6 (1996); M. Ueda and A. J. Leggett, *ibid.* **80**, 1576 (1998); E. J. Mueller and G. Baym, Phys. Rev. A **62**, 053605 (2000).

[9] F. Dalfovo and S. Stringari, Phys. Rev. A **53**, 2477 (1996); R. J. Dodd, J. Res. Natl. Inst. Stand. Technol. **101**, 545 (1996); T. J. Alexander and L. Bergé, Phys. Rev. E **65**, 026611 (2002); H. Saito and M. Ueda, Phys. Rev. A **69**, 013604 (2004); D. Mihalache, D. Mazilu, B. A. Malomed, and F. Lederer, *ibid.* **73**, 043615 (2006); L. D. Carr and C. W. Clark, Phys. Rev. Lett. **97**, 010403 (2006).

[10] N. K. Wilkin, J. M. F. Gunn, and R. A. Smith, Phys. Rev. Lett. **80**, 2265 (1998); B. Mottelson, *ibid.* **83**, 2695 (1999); C. J. Pethick and L. P. Pitaevskii, Phys. Rev. A **62**, 033609 (2000).

[11] E. Lundh, A. Collin, and K.-A. Suominen, Phys. Rev. Lett. **92**, 070401 (2004).

[12] G. M. Kavoulakis, A. D. Jackson, and G. Baym, Phys. Rev. A **70**, 043603 (2004); A. Collin, *ibid.* **73**, 013611 (2006).

[13] A. Collin, E. Lundh, and K.-A. Suominen, Phys. Rev. A **71**, 023613 (2005); S. Bargi, G. M. Kavoulakis, and S. M. Reimann, *ibid.* **73**, 033613 (2006).

[14] Y. J. He, B. A. Malomed, D. Mihalache, and H. Z. Wang, Phys. Rev. A **78**, 023824 (2008).

[15] A. Snyder and J. Mitchell, Science **276**, 1538 (1997).

[16] V. M. Pérez-García, H. Michinel, J. I. Cirac, M. Lewenstein, and P. Zoller, Phys. Rev. A **56**, 1424 (1997).

[17] B. A. Malomed, in *Progress in Optics*, edited by E. Wolf (North-Holland, Amsterdam, 2002), Vol. 43, p. 71.

[18] M. L. Chiofalo, S. Succi, and M. P. Tosi, Phys. Rev. E **62**, 7438 (2000).

[19] H. Sakaguchi and H. Takeshita, J. Phys. Soc. Jpn. **77**, 054003 (2008).

[20] S. Komineas, N. R. Cooper, and N. Papanicolaou, Phys. Rev. A **72**, 053624 (2005).

[21] M. Desaix, D. Anderson, and M. Lisak, J. Opt. Soc. Am. B **8**, 2082 (1991).

[22] U. R. Fischer, Phys. Rev. Lett. **93**, 160403 (2004).

[23] B. B. Baizakov, B. A. Malomed, and M. Salerno, Phys. Rev. A **70**, 053613 (2004); H. Sakaguchi and B. A. Malomed, *ibid.* **75**, 063825 (2007).

[24] D. Yoshioka, *The Quantum Hall Effect* (Springer-Verlag, Berlin, 2002).